Characteristics of P, SV, and SH wave propagation in an anisotropic medium

Amber C. Kelter and John C. Bancroft

ABSTRACT

Two methods of approximating phase and group velocities in an anisotropic medium are explored. Wavefront shapes and expected diffractions from a scatterpoint are investigated. It was found that the popular approximations given by Thomsen in 1986 lose accuracy when compared to more exact solutions; this is especially evident for the case of SV-waves.

INTRODUCTION

Most models in exploration seismology presume that the earth is isotropic — that is, seismic velocities do not vary with direction. However, individual crystals and most common earth materials are observed to be anisotropic with elastic parameters that vary with orientation. Thus, it would be surprising if the earth was completely isotropic. It seems that seismologists have been somewhat cautious in considering the full effects of anisotropy. There are many reasons for this, including the greater computational complexity and lack of computing power, the difficulty of inverting data for a larger number of elastic constants, and in some cases, a lack of compelling evidence for the existence of anisotropy. However, lately it has become apparent that anisotropy is evident in many parts of the earth and therefore anisotropic studies are becoming an increasingly important aspect of seismological research (Shearer, 1999).

REVIEW OF ANISOTROPY

Hooke's law was formulated by Love (1927). When an elastic wave propagates through rocks the displacements are in accordance with Hooke's Law namely the stress and strain are related through a constitutive relation that can be written as

$$\sigma_{ij} = c_{ijkl}e_{kl}, \tag{1}$$

where σ_{ij} is the stress tensor, c_{ijkl} is the elastic tensor and e_{kl} is the strain tensor. Both the stress and the strain are symmetric. Using the Voigt recipe (Musgrave, 1970) the fourth-order stiffness tensor can be rewritten as a second-order symmetric matrix:

$$c_{ijkl} \Rightarrow c_{\alpha\beta}, \tag{2}$$

where $ij \Rightarrow \alpha$ and $kl \Rightarrow \beta$.

In an isotropic medium, the elastic tensor is written as

$$
c_{\alpha\beta} =
\begin{bmatrix}
c_{33} & c_{33}-2c_{44} & c_{33}-2c_{44} & 0 & 0 & 0 \\
c_{33}-2c_{44} & c_{33} & c_{33}-2c_{44} & 0 & 0 & 0 \\
c_{33}-2c_{44} & c_{33}-2c_{44} & c_{33} & 0 & 0 & 0 \\
0 & 0 & 0 & c_{44} & 0 & 0 \\
0 & 0 & 0 & 0 & c_{44} & 0 \\
0 & 0 & 0 & 0 & 0 & c_{44}
\end{bmatrix}.
\tag{3}
$$

The components of the isotropic elastic tensor are related to the lamé parameters λ and μ by

$$
c_{33} = \lambda + 2\mu,
\tag{4a}
$$

and

$$
c_{44} = \mu .
\tag{4b}
$$

The two Lamé parameters completely describe the linear stress-strain relation within an isotropic solid. For a transverse isotropic medium with a vertical symmetry axis (VTI medium), the elastic tensor is written as (Thomsen, 1986)

$$
c_{\alpha\beta} =
\begin{bmatrix}
c_{11} & c_{11}-2c_{66} & c_{13} & 0 & 0 & 0 \\
c_{11}-2c_{66} & c_{11} & c_{13} & 0 & 0 & 0 \\
c_{13} & c_{13} & c_{33} & 0 & 0 & 0 \\
0 & 0 & 0 & c_{44} & 0 & 0 \\
0 & 0 & 0 & 0 & c_{44} & 0 \\
0 & 0 & 0 & 0 & 0 & c_{66}
\end{bmatrix}.
\tag{5}
$$

The tensor now has five independent elastic constants that describe the medium. The introduction of three new components or elastic moduli is significant. These elastic components are related to the anisotropic or Thomsen's parameters and are developed below.

PHASE VELOCITY

The phase velocities for three mutually orthogonal polarizations can be described in terms of the elastic constants (Thomsen, 1986). Daley and Hron (1977) give expressions for the phase velocities in terms of the elastic tensor components. The phase velocity of a compressional wave is

$$
v_P(\theta) = \sqrt{\frac{c_{33}+c_{44}+(c_{11}-c_{33})\sin^2(\theta)+D(\theta)}{2\rho}} .
\tag{6}
$$

The phase velocity of a shear wave with a vertical polarization direction is expressed as

$$v_{SV}(\theta) = \sqrt{\frac{c_{33} + c_{44} + (c_{11} - c_{33})\sin^2(\theta) - D(\theta)}{2\rho}} \ , \tag{7}$$

and the shear velocity with horizontal polarization is expressed as

$$v_{SH}(\theta) = \sqrt{\frac{c_{66}\sin^2(\theta) + c_{44}\cos^2(\theta)}{\rho}} \ , \tag{8}$$

where ρ is the density and the symbol $D(\theta)$ denotes

$$D(\theta) = \{(c_{33} - c_{44})^2 + 2[2(c_{13} - c_{44})^2 - (c_{33} - c_{44})(c_{11} + c_{33} - 2c_{44})]\sin^2\theta +$$
$$[(c_{11} + c_{33} - 2c_{44})^2 + 4(c_{13} - c_{44})^2]\sin^4\theta\}^{1/2}. \tag{9}$$

It is convenient to define the non-dimensional anisotropic parameters in terms of the elastic tensor components and express Equations (6) to (8) in terms of these. From Thomsen (1986), the anisotropic parameters are defined as

$$\varepsilon = \frac{c_{11} - c_{33}}{2c_{33}} \ , \tag{10}$$

$$\gamma = \frac{c_{66} - c_{44}}{2c_{44}} \ , \tag{11}$$

and

$$\delta = \frac{(c_{13} + c_{44})^2 - (c_{33} - c_{44})^2}{2c_{33}(c_{33} - c_{44})} \ . \tag{12}$$

If the velocities in the direction of the symmetry axis are defined as

$$\alpha_0 = \sqrt{c_{33}/\rho} \tag{13}$$

for the P-wave velocity and as

$$\beta_0 = \sqrt{c_{44}/\rho} \tag{14}$$

for the S-wave velocity then Equations (10)–(14) now constitute five linear equations with five unknowns that are solved such that

$$c_{33} = \rho\alpha_0^2 \text{,} \tag{15}$$

$$c_{44} = \rho\beta_0^2 \text{,} \tag{16}$$

$$c_{11} = \varepsilon 2c_{33} + c_{33} = 2\rho\alpha_0^2(\varepsilon + \frac{1}{2}) \text{,} \tag{17}$$

$$c_{66} = \gamma 2c_{44} + c_{44} = 2\rho\beta_0^2(\gamma + \frac{1}{2}) \text{,} \tag{18}$$

and

$$c_{13} = \sqrt{\delta 2c_{33}(c_{33-}c_{44}) - (c_{33-}c_{44})^2} - c_{44}$$

$$c_{13} = \sqrt{\delta\rho\alpha_0^2(\rho\alpha_0^2 - \rho\beta_0^2) - (\rho\alpha_0^2 - \rho\beta_0^2)^2} - \rho\beta_0^2$$

$$c_{13} = \rho\alpha_0\sqrt{(\alpha_0^2 - \beta_0^2)(2\delta + 1 - \frac{\beta_0^2}{\alpha_0^2})} - \rho\beta_0^2 \tag{19}$$

Substitute these solutions into Equations (6)–(8). Developing into Taylor series and neglecting higher order terms we get solutions (Equations (20a), (21a), and (22a)) for the phase velocities that are valid under the condition of weak anisotropy. Equations (20b), (21b) and (22b) show results without simplifications (Daley and Hron, 1977). The accuracy of these approximations is investigated below: Figures 3, 6, and 9. Note for simplicity group velocity are only going to be calculated from the Taylor-series approximations (Equations (20a), (21a) and (22a)).

$$v_P(\theta) = \alpha_0(1 + \delta\sin^2\theta\cos^2\theta + \varepsilon\sin^4\theta) \text{,} \tag{20a}$$

$$v_p(\theta) = \alpha\sqrt{1 + \varepsilon\sin^2\theta + \frac{1}{2}\left(1 + \frac{\beta^2}{\alpha^2}\right)\left\{\sqrt{1 + \frac{4(2\delta - \varepsilon)\sin^2\theta\cos^2\theta}{1 + \frac{\beta^2}{\alpha^2}} + \frac{4\varepsilon\left(1 - \frac{\beta^2}{\alpha^2} + \varepsilon\right)\sin^4\theta}{\left(1 + \frac{\beta^2}{\alpha^2}\right)^2}} - 1\right\}} \tag{20b}$$

$$v_{SV}(\theta) = \beta_0(1 + \frac{\alpha_0^2}{\beta_0^2}(\varepsilon - \delta)\sin^2\theta\cos^2\theta) \text{,} \tag{21a}$$

$$v_{sv}(\theta) = \beta\sqrt{1 + \frac{\alpha^2}{\beta^2}\left[\varepsilon\sin^2\theta - \frac{1}{2}\left(1 - \frac{\beta^2}{\alpha^2}\right)\left\{\sqrt{1 + \frac{4(2\delta - \varepsilon)\sin^2\theta\cos^2\theta}{1 + \frac{\beta^2}{\alpha^2}} + \frac{4\varepsilon\left(1 - \frac{\beta^2}{\alpha^2} + \varepsilon\right)\sin^4\theta}{\left(1 + \frac{\beta^2}{\alpha^2}\right)^2}} - 1\right\}\right]} \tag{21b}$$

and

$$v_{SH}(\theta) = \beta_0^2 (1 + \gamma \sin^2 \theta),$$
(22a)

$$v_{SH}(\theta) = \beta_0 \sqrt{1 + \gamma \sin^2 \theta}.$$
(22b)

GROUP VELOCITY

The x and y axes are equivalent for a transversely isotropic medium, therefore we can confine ourselves to the x-z plane in the discussion of a VTI medium. Figure 1 depicts the phase angle, θ, the ray or group angle, ϕ, and the phase velocity, $v(\theta)$, and the group velocity, $V(\phi)$. The group velocity is the velocity of the ray and represents the direction of energy transport. In contrast, the phase velocity is the local velocity of the wavefront in the direction perpendicular to the wavefront and is the velocity used when talking about the slowness or ray parameter, p.
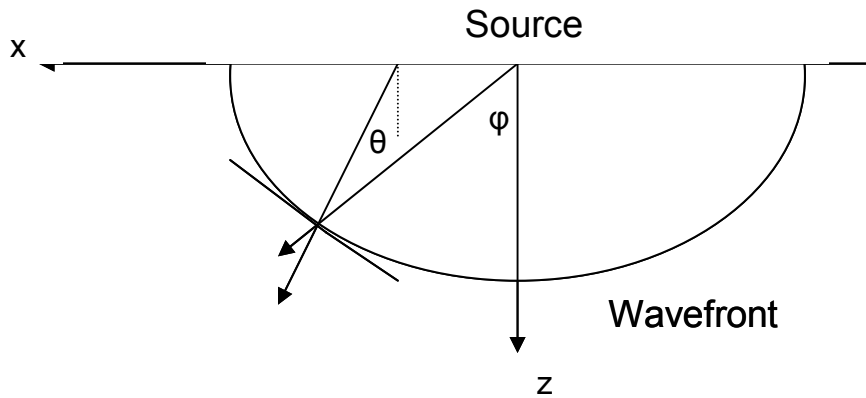

FIG. 1. Depiction of the phase and group velocities. Note that the angle is measured with respect to the vertical axis (symmetry axis). The group velocity is the direction of energy propagation while the phase velocity is the local velocity of the wavefront.

For a plane wave, the phase velocity is described as $v = \dfrac{\omega}{k}$ where ω is the angular frequency and k is the wavenumber. If $\vec{k} = k(\sin\theta \hat{x}_1 + \cos\theta \hat{x}_3)$ then the phase velocity as function of the angle is given by

$$v(\theta) = \frac{\omega}{k}(\sin\theta \hat{x}_1 + \cos\theta \hat{x}_3).$$
(23a)

However, it is the group velocity, the velocity at which the energy propagates, that would be measured at a geophone. The group velocity is defined as $V(\phi) = \dfrac{d\omega}{dk}$ or in terms of the phase velocity as

$$V(\phi) = \left(v\sin\theta + \frac{dv}{d\theta}\cos\theta \right)\hat{x}_1 + \left(v\cos\theta - \frac{dv}{d\theta}\sin\theta \right)\hat{x}_3. \qquad (23b)$$
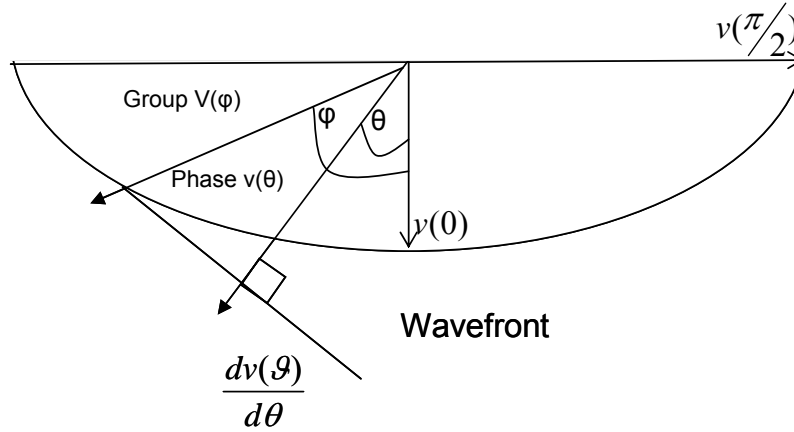

FIG. 2. Depiction of the phase and group velocities used to define the group velocity from the phase velocity.

From Figure 2 and Byun (1984) it is evident that

$$v(\theta) = V(\phi)\cos(\phi - \theta), \qquad (24)$$

$$\tan(\phi - \theta) = \frac{1}{v(\theta)}\frac{dv(\theta)}{d\theta}, \qquad (25)$$

and

$$V^2(\phi) = v^2(\theta) + \left(\frac{dv}{d\theta} \right)^2. \qquad (26)$$

Therefore, the magnitude of the group velocity can be defined in terms of the phase velocity and the phase angle. In order to solve for the group angle, we need to apply the trigonometric identity in Equation (27) to Equation (25)

$$\tan(x - y) = \frac{\tan(x) - \tan(y)}{1 + \tan(x)\tan(y)}. \qquad (27)$$

Upon solving for the group angle, ϕ, we get a solution

$$\phi = \tan^{-1}\left[\frac{\tan(\theta) + \dfrac{1}{v(\theta)}\dfrac{dv(\theta)}{d\theta}}{1 - \dfrac{1}{v(\theta)}\dfrac{dv(\theta)}{d\theta}\tan(\theta)} \right]. \qquad (28)$$

We have now successfully defined the group velocity and its angle.

WEAK ANISOTROPIC APPROXIMATION

Thomsen (1984) introduced an approximation to the methods described above to go from phase velocity (Equations (20a), (21a) and (22a)) to group velocity and corresponding group angle. He stated that a sufficient linear approximation is

$$V(\phi) = v(\theta),$$
(29)

and that the group angle could be solved from the linear approximation

$$\tan(\phi) = \tan(\theta)\left[1 + \frac{1}{\sin(\theta)\cos(\theta)} \frac{1}{v(\theta)} \frac{dv}{d\theta}\right].$$
(30)

This leads to group angles indicated by Equations (31)–(33) for the P and two S waves

$$\tan(\phi_P) = \tan(\theta)\left[1 + 2\delta + 4(\varepsilon - \delta)\sin^2(\theta)\right],$$
(31)

$$\tan(\phi_{SV}) = \tan(\theta)\left[1 + 2\frac{\alpha_0^2}{\beta_0^2}(\varepsilon - \delta)(1 - 2\sin^2(\theta))\right],$$
(32)

and

$$\tan(\phi_{SH}) = \tan(\theta)(1 + 2\gamma).$$
(33)

Solving for the group velocity using Equation (26) we get a solution that is quadratic in anisotropy. If the higher order terms are neglected the linear approximation goes as

$$\begin{aligned} V_P(\phi) &= v_p(\theta) \\ V_{SV}(\phi) &= v_{SV}(\theta) \\ V_{SH}(\phi) &= v_{SH}(\theta) \end{aligned}$$
(34)

thereby validating Equation (29). The above formula states that if the phase velocity and phase angle are given, the approximate group angle can be solved for from Equations (31)–(33) and the approximate magnitude of the group velocity can be solved using Equations (20a), (21a), and (22a).

ANISOTROPY PARAMETERS

For most sedimentary rocks, the parameters ε, γ, and δ are of the same order of magnitude and usually much less than 0.2; further for most rock types the anisotropy parameters are positive (Thomsen, 1986). However, it is not unheard of to have negative values for the anisotropy parameters. In the modelling that follows the parameters are pushed to their limits to explore the boundaries of "common" rock types. When the special case of horizontal incidence is considered, we can develop a physical meaning for the anisotropic parameters ε and γ. If, in equations (20a) and (22a), we let the angle equal 90 degrees and solve for the parameter, we obtain $\varepsilon = \frac{\alpha_h - \alpha_0}{\alpha_0}$ and $\gamma = \frac{\beta_h - \beta_0}{\beta_0}$, where α_h and β_h are the horizontal P- and S-wave velocities respectively. In particular these

parameters are a measure of the anisotropic behaviour of a rock and are a calculation of the fractional difference between the horizontal and vertical velocities. It is much more difficult to gain a physical understanding of the third parameter other than to say that, it is a critical factor that controls the near vertical response, and that it determines the shape of the wavefront.

VALIDITY OF THE WEAK ANISOTROPIC APPROXIMATION

Comparison of the approximations given by Thomsen (1986) to the more accurate equations for the group velocity shows that the approximation is only valid out to about 30 degrees for incident angle of SV-waves and appears to always be valid for the P and SH-wave. Figures 3, 4, 6, 7, 9, and 10 show the phase velocity and the group velocity calculated from the more exact expression and from the anisotropic approximation for the three different wave polarizations. The figures demonstrate the shape of the expected wavefront and are essentially the velocity plotted in polar format.
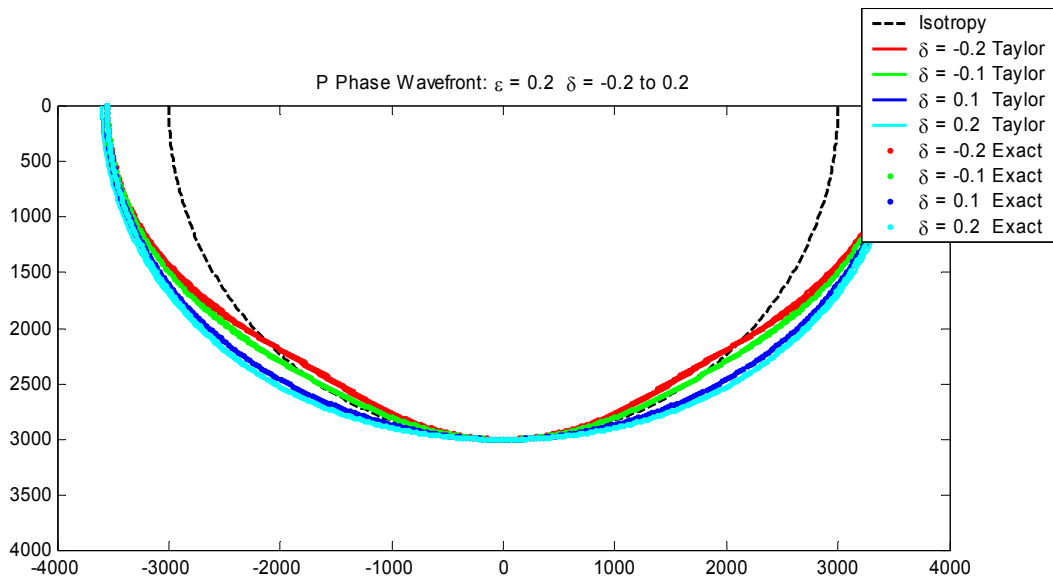

FIG. 3. P-wave phase wavefront. Epsilon is constant at 0.2 and delta varies from -0.2 to 0.2. The isotropic response is shown as the thick dashed black line. It is seen that the exact expression (Daley and Hron, 1977) and the Taylor series truncated expression (Thomsen, 1986) are very similar.

Figure 3 reveals the expected wavefront shape for the P-wave phase velocity. Epsilon (ϵ) is equal to 0.2 and delta (δ) is varied from -0.2 to 0.2. When $\delta=\epsilon$ we get what is commonly referred to as elliptical anisotropy (Yilmaz, 2001). As one might infer, the wavefront in this case is elliptical in shape. When delta is negative, we get a crossing over with respect to the isotropic response which is shown, indicated by the thick dashed black line. Also note that the horizontal P-wave velocity is always greater than the vertical P-wave velocity. The more exact expression for the phase velocity response is nearly identical to the approximated Taylor-series expression and hence the Taylor series is a good approximation to the more complicated expression. As mentioned above, only the Taylor series response is considered when calculating group velocities.
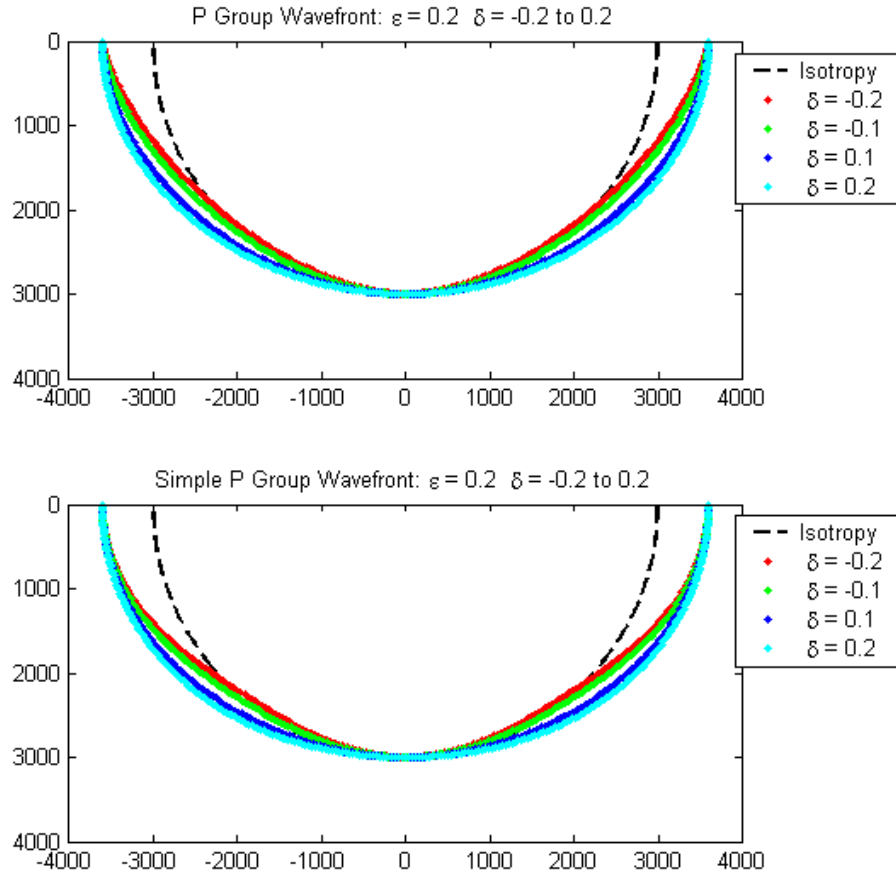
FIG. 4. P-wave group wavefront. Epsilon is constant at 0.2 and delta varies from -0.2 to 0.2. Upper image is calculated from the more exact expressions while the lower image is calculated from the anisotropic approximation.

Figure 4 shows the P-wave group wavefront. Again, when ε=δ we see an elliptical response. The upper image is the response from the more exact expression while the lower image is the response to the approximated expression. Inspection of the two shows that they are vastly similar and that the approximated expression appears to be valid at all incident angles; a closer look is seen in Figure 5 where the difference has been taken between the more exact expression and its approximation.

Difference between the P-wave complete velocity expression and the anisotropic approximation
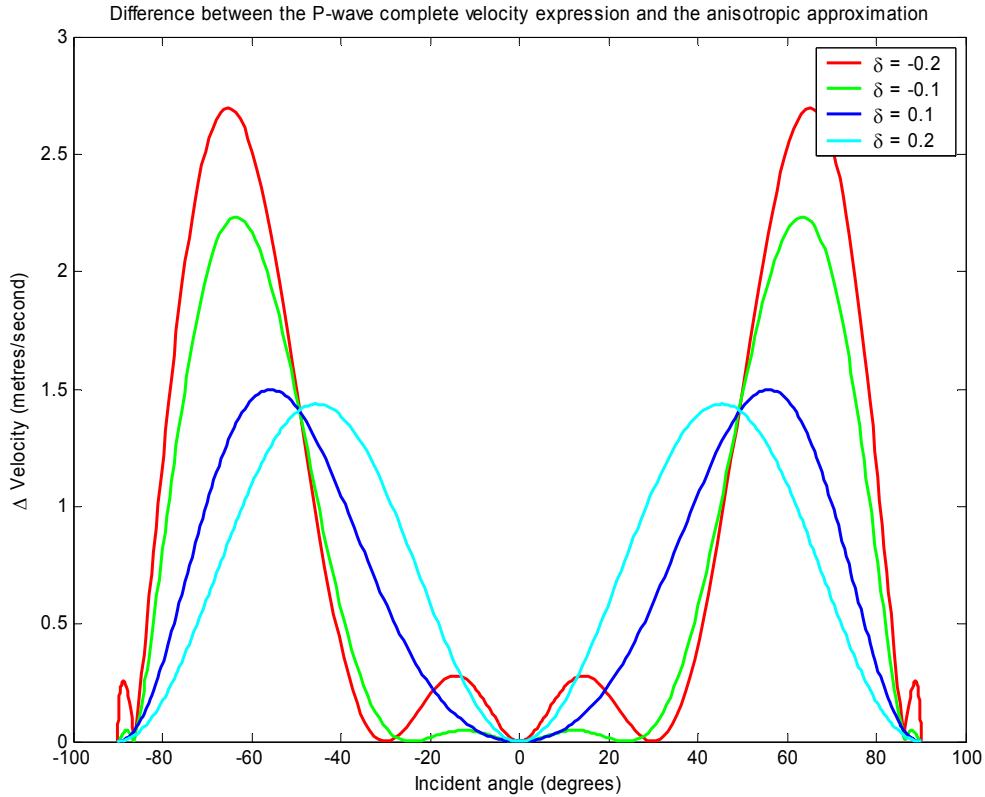

FIG. 5. The difference between the more exact expression for the P-wave group velocity and the approximation for the P-wave group velocity as a function of angle.

As the value of delta deviates more from zero, the approximation becomes less accurate. For positive delta values, the greatest deviation occurs at relatively smaller incident angles as the value of delta increases in magnitude. When the delta value has a negative sign, the angle of greatest deviation also shifts to a slightly smaller incident angle for delta values that are greater in magnitude. Further, when the value is negative, we see a difference as large as 88 metres/second at about a 50-degree incident angle for a delta value of -0.2. In actuality, this only corresponds to an approximately 2.77% deviation in velocity for the model used here.
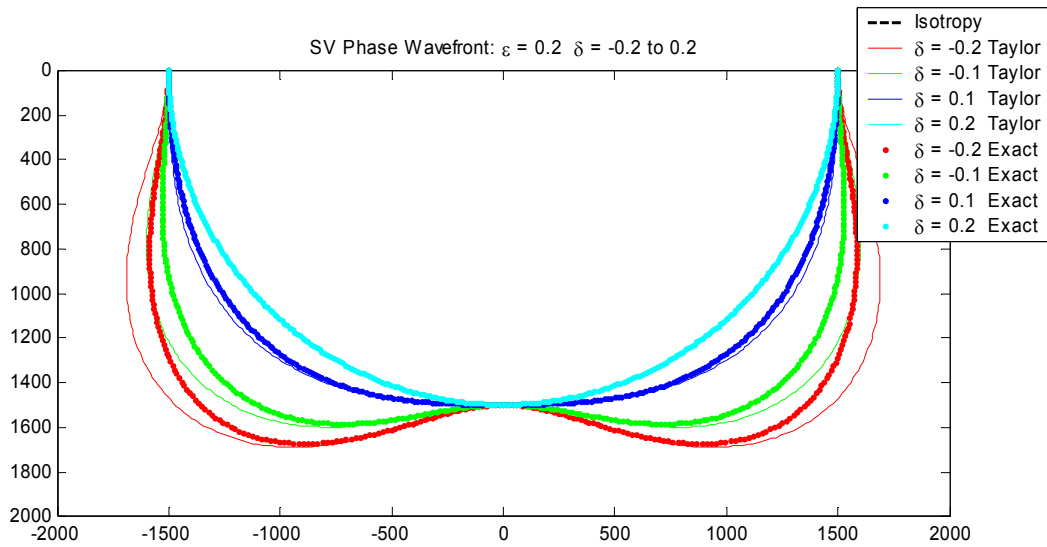
FIG. 6. SV-wave phase wavefront. Epsilon is constant at 0.2 and delta varies from -0.2 to 0.2. There is an obvious difference between the exact response and the approximated response for negative delta values.

For the SV-wave phase velocity, we see that negative delta values cause a significant bulging response at around 45 degrees with respect to the isotropic response; and, interestingly, it is observed that the response, whether the delta value is positive or negative, is always greater than the isotropic response. There is an immediate difference between the exact expression and the Taylor series expression for negative delta values, showing that the approximation loses validity for the SV-wave; however, as mentioned above, only the Taylor series response is considered when calculating group velocities as this is the formulation that is commonly.
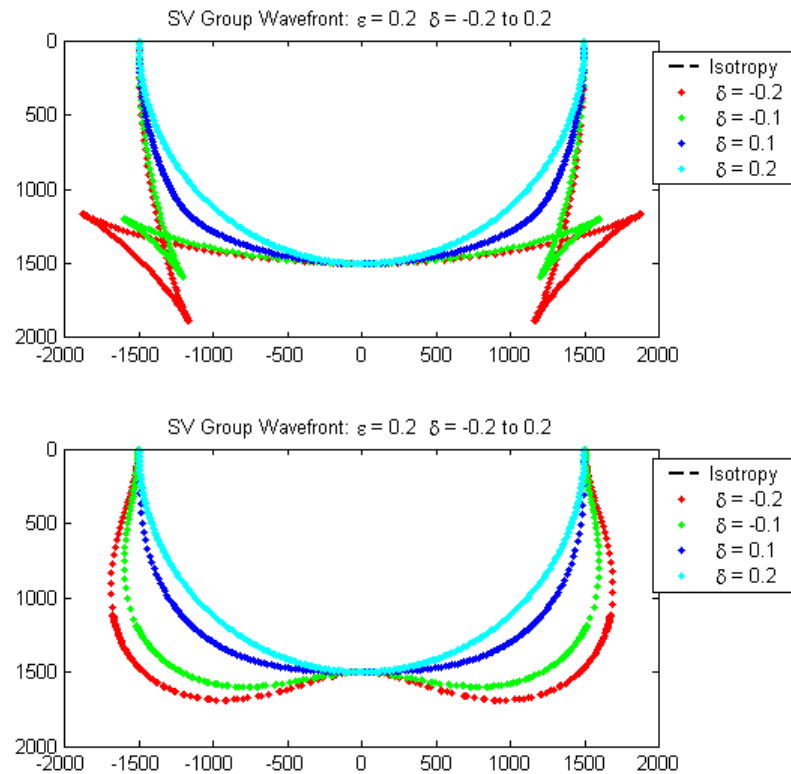
FIG. 7. SV-wave group wavefront. Epsilon is constant at 0.2 and delta varies from -0.2 to 0.2. The upper image is calculated from the more exact expressions while the lower image is calculated from the anisotropic approximation.

The more exact expression for the SV-wave group wavefront response is seen in the top image in Figure 7, and the approximation in the lower image. For the SV-waves, we observe that the approximation seems to fail at about 30 degrees or so; this is also evident in Figure 8. Most notable is that the cusps or triplications that are sometimes seen in the more exact expression are not picked up by the approximation. The most extreme deviation is observed at about 70 degrees where, for a delta value of -0.2, the velocity difference is over 700 metres/second, corresponding to a 44% error in the calculation of the group velocity at this point. The difference between the more exact and approximate is seen in Figure 8.
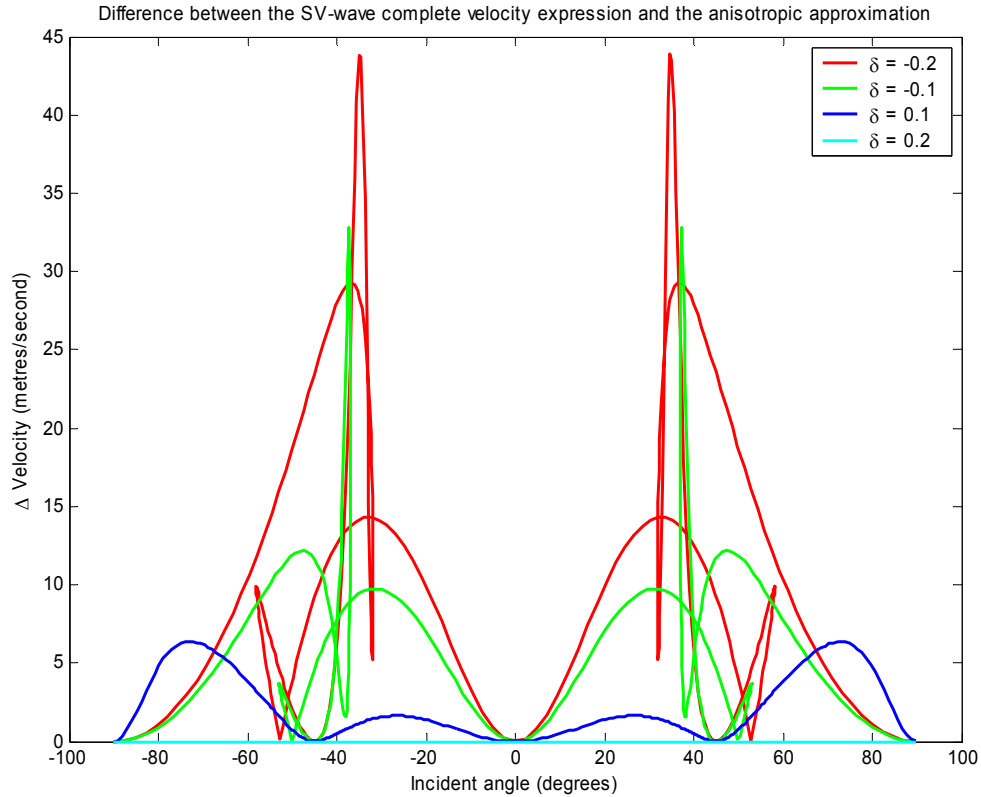
FIG. 8. The difference between the more exact expression for the SV-wave group velocity and the approximation for the SV-wave group velocity as a function of angle.

Examination of Figure 8 tells us that negative delta values produce far less accurate results than positive delta values, and that, at an angle of roughly 60 degrees, the approximation is nearly identical to the more exact solution. As the magnitude of a negative delta value decreases, the point of minimum accuracy corresponds to a smaller angle.
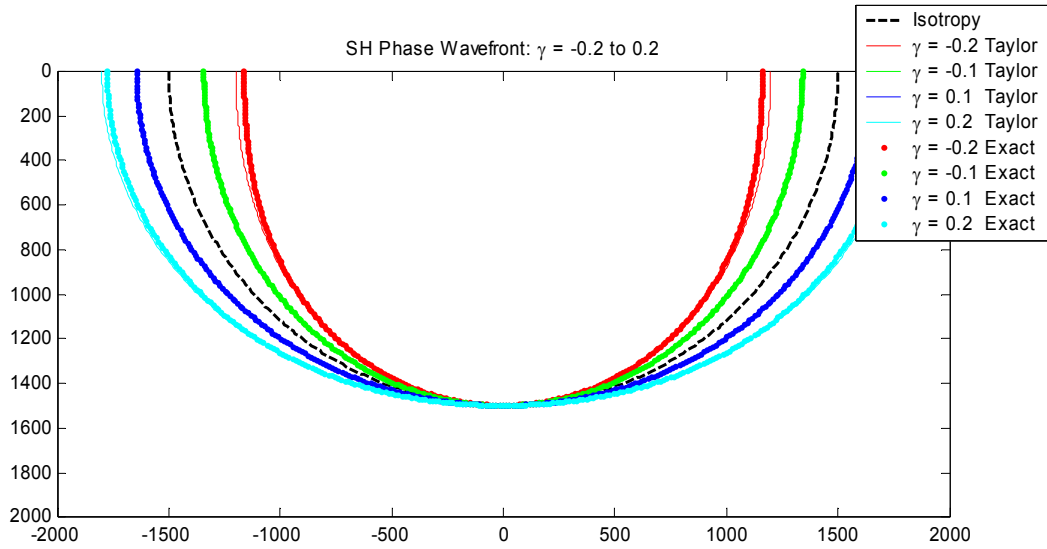
FIG. 9. SH-wave phase wavefront. Gamma varies from -0.2 to 0.2. The exact expression and the truncated Taylor-series approximation are similar.

In the SH-wave phase velocity case, we observe that negative gamma values produce results that are smaller that the isotropic case, while positive values produce results that are larger than would be found in the isotropic case. For the SH-wave the result is always elliptical. The exact response and the Taylor series response exhibit nearly identical characteristics. Thus the Taylor series is a good approximation to the more complicated expression. As mentioned above, only the Taylor series response is considered when calculating group velocities.
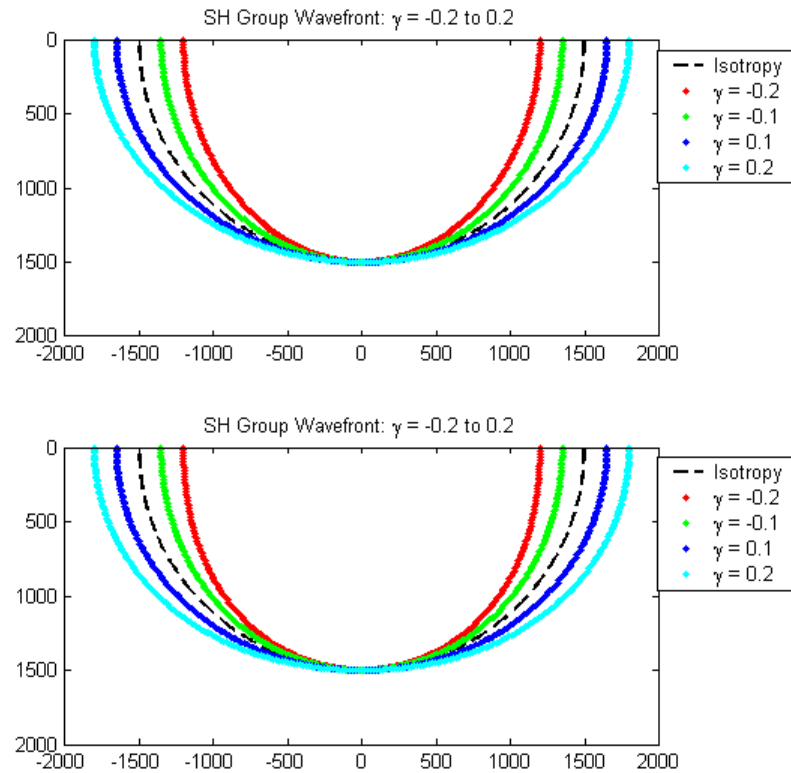
FIG. 10. SH-wave group wavefront. Gamma varies from -0.2 to 0.2. The upper image is calculated from the more exact expressions, while the lower image is calculated from the anisotropic approximation.

Similar trends are observed for the SH-wave group velocities as are observed for the SH-wave phase velocity. On first inspection, the results of the more exact (Figure 10, top) and approximation (Figure 10, bottom) look similar. Figure 11 shows a more in-depth look at the difference between the two results.
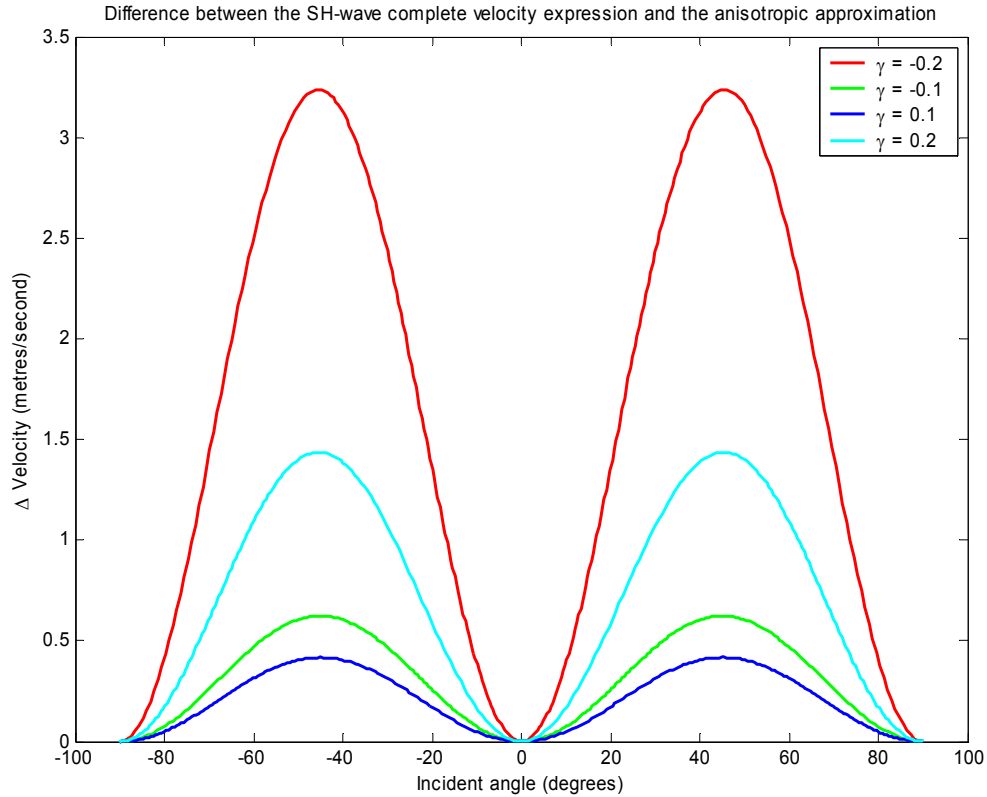
FIG. 11. The difference between the more exact expression for the SH-wave group velocity and the approximation for the SH-wave group velocity as a function of angle.

The approximation always gives an answer that is larger relative to the more exact solution. The largest deviation is seen at 75 degrees. For a delta value of -0.2, the velocity is in error by 43 m/s; this corresponds to a difference of 3.2%. The SH-wave approximation will produce adequate results for all incident angles unlike the SV-wave approximation.

In all cases, it is the magnitude of the delta or gamma value that determines the inaccuracy of the approximation, with values that are greater in magnitude creating less accurate results. Negative values always produce more inaccurate results. Both of the solutions for the group velocity converge at zero and ninety degrees of incidence. This again is consistent with all three possible polarizations.

FROM GROUP VELOCITY TO DIFFRACTIONS

The group velocity at a certain incident angle can be used to calculate the two-way traveltime to a scatterpoint a certain depth. Once the two-way traveltime is found, the expected diffraction shape from the scatterpoint can be put forward (see Figure 12).

Group
Wavefront &
Ray

x

z

ϕ

Ray & Scatterpoint
(Traveltime Defined)

x

z
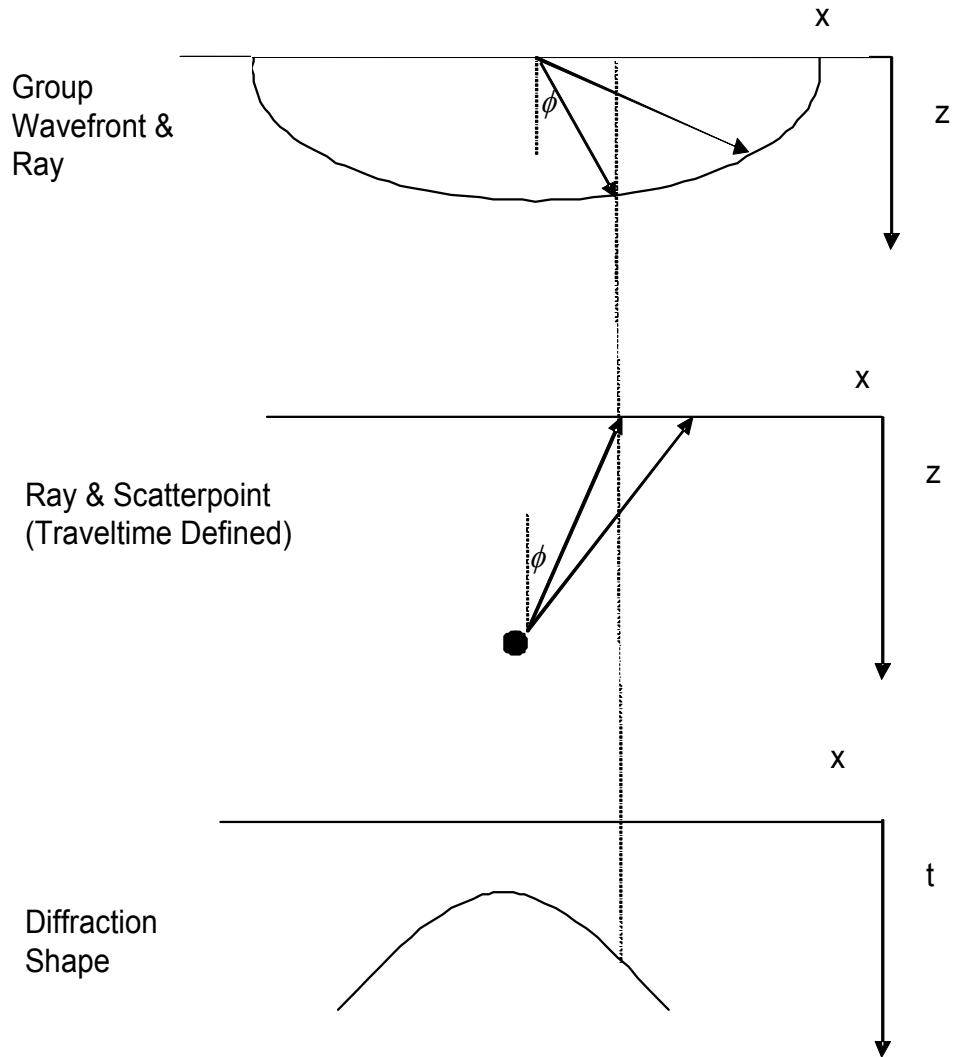
ϕ

Diffraction
Shape

x

t

FIG. 12. If the group velocity as a function of incidence angle is known, the two-way traveltime to a scatterpoint at depth can be calculated. The two-way traveltime can be used to predict the diffraction that would be expected from the scatterpoint.

The expected diffraction shapes from a scatterpoint located at a depth of 500 metres was calculated for the three different wave polarizations and are seen in Figures 12–15.
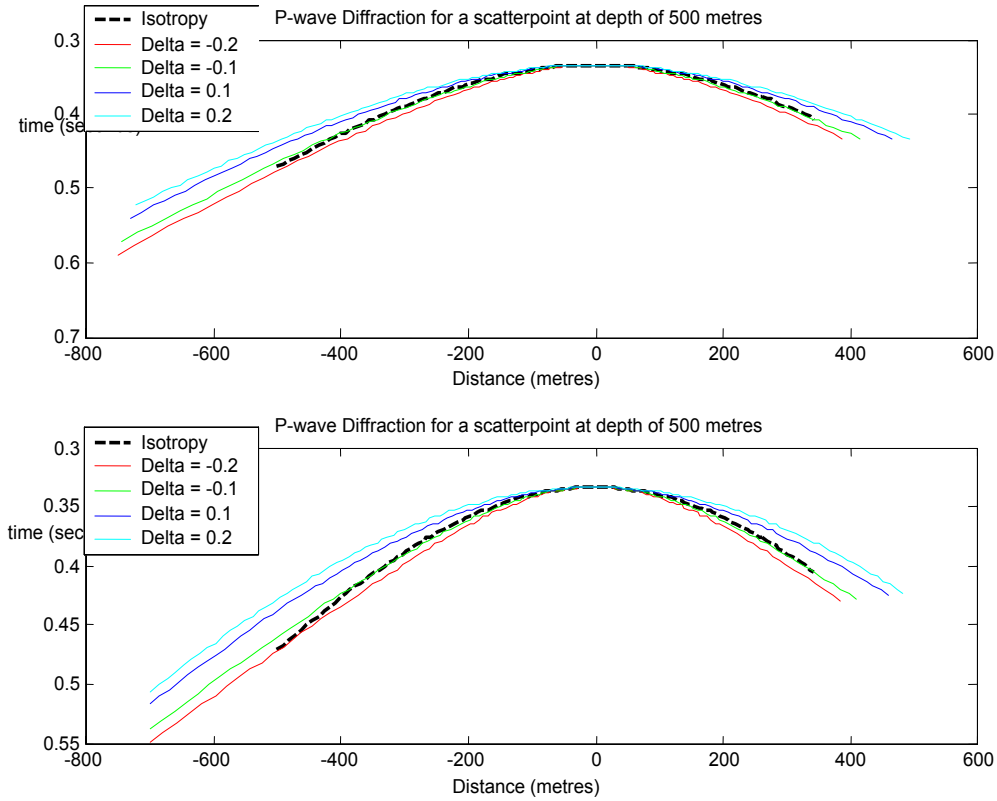
FIG. 13. P-wave diffractions from a scatterpoint located at a depth of 500 metres. The top part is the more exact solution, while the bottom part is calculated from the approximation. The left hand side has been calculated out to 45 degees, while the right-hand side has been calculated out to 30 degrees for the incidence angle.

Both images in Figure 13 suggest that hyperbolic moveout could be applied, as both the more exact solution (top) and the approximation (bottom) produce results that appear to be hyperbolic in shape. The left-hand side of the diffraction has been calculated out to 45 degrees while the right hand side has been calculated to 30 degrees. The reasons for doing this will become obvious shortly. Note the slight difference in the two methods at 500 metres, where one can see that the approximation is deviating from the more exact solution.
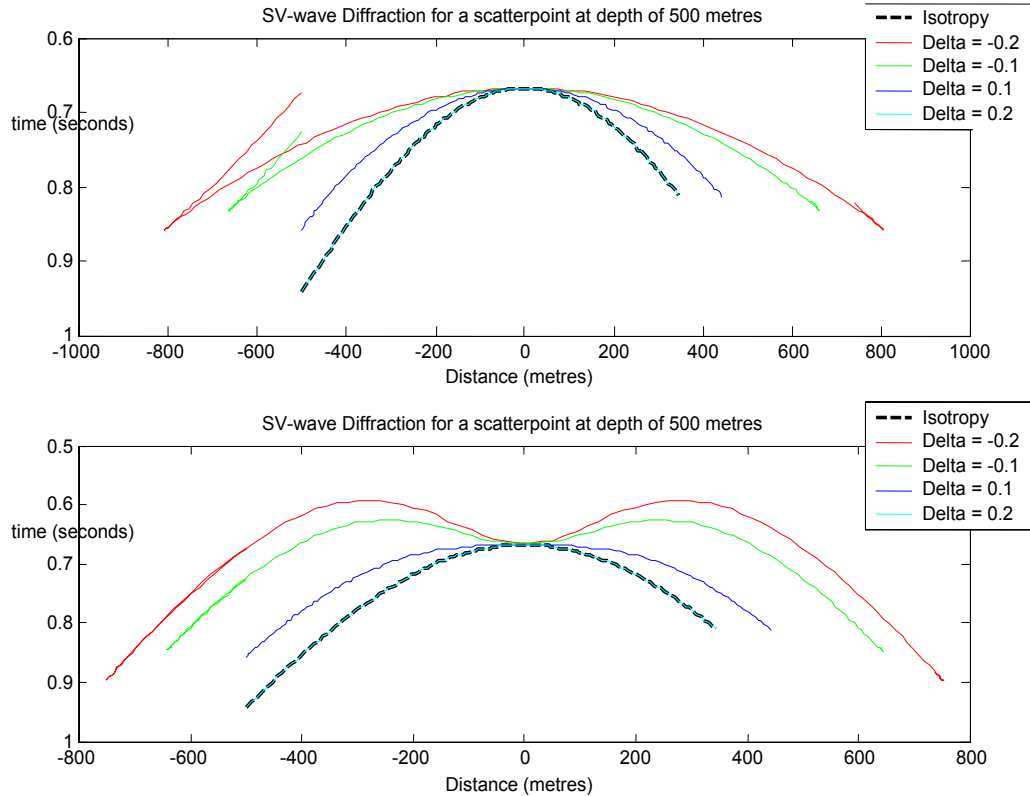
FIG. 14. Expected SV-wave diffraction for a scatterpoint at 500 metres. The top image is calculated from the more exact solution and the bottom from the approximation. The left-hand side has been calcultated out to 45 degees while the right-hand side has been calculated out to 30 degrees for the incidence angle.

Inspection of Figure 14 suggests that the anisotropic approximation will not allow for conventional hyperbolic moveout to be applied. On the other hand, the more exact solution exhibits a nearly hyperbolic response to a scatterpoint at depth. Focusing on the top image we see that the result is roughly hyperbolic out to 30 degrees. There is a slight deviation at the tip when delta = -0.2, but recall that this value is on the border of strong/weak anisotropy and the methods presented in this paper are relevant only under weakly anisotropic conditions. The response when the delta values are all positive for the more exact solution suggests that the response is hyperbolic all the way out to 45 degrees.
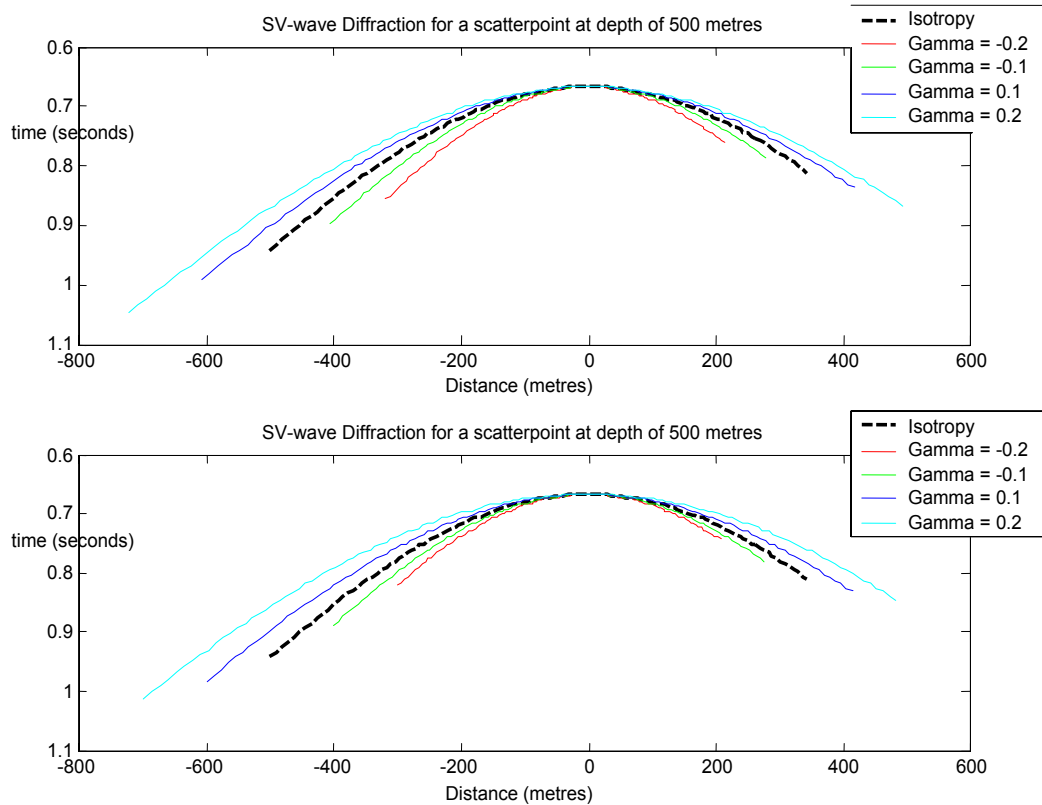
FIG. 15. Diffractions for a scatterpoint from the SH-wave. All responses for the SH-wave are hyperbolic in shape. The left-hand side has been calculated out to 45 degees while the right-hand side has been calculated out to 30 degrees for the incidence angle.

Figure 15 shows that the expected diffraction from a scatterpoint at depth for the SH-wave will produce results that are hyperbolic in shape and consequently traditional processing can still be applied to this case. The results are valid for hyperbolic moveout all the way out to 45 degrees.

Expected diffractions from converted-wave data is also modelled for a scatterpoint located at 500 metres. A ray emitted as a P-wave with a phase angle θ_p from the surface reflects as an S-wave with angle θ_s. The two angles are related by Snell's law

$$p = \frac{\sin\theta_p}{v_p} = \frac{\sin\theta_s}{v_s},$$

(35)

where p is the ray parameter. Note that the subsurface area illuminated by this ray differs from the midpoint between the source and receiver that would have been highlighted in a PP survey by a distance that is dependant on $G = \dfrac{V_p}{V_s}$ (Tessmer and Behle, 1988). Thus the reflection point can not be determined with geometrical tactics. PS data-processing is more critically dependant on physical properties than is PP data-processing.
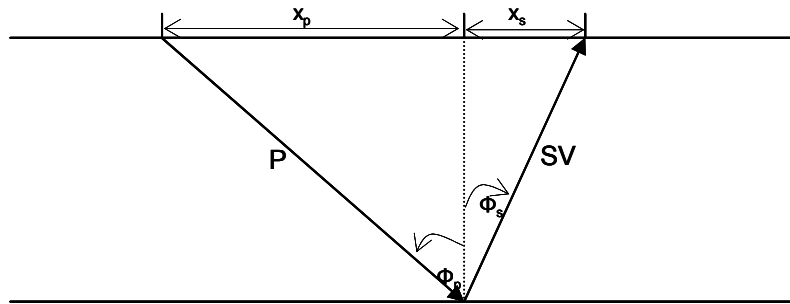
FIG. 16. Depiction of a PS survey. The surface area highlighted is no longer equivalent to the source receiver midpoint, but is dependent on Vp/Vs.

The algorithm for determining expected diffraction shapes of converted waves (C-waves) is such that the P-wave part of the solution is determined similarly to the PP case. The phase angle and velocity corresponding to the first leg of the solution are then used to calculate the ray parameter. The slowness parameter is next calculated for a range of shear phase angles, and a matching scheme implemented to choose the best angle such that the ray parameter is preserved. The group angle and velocity are calculated and the traveltime for the second leg of the C-wave determined. Results are seen in Figure 17.
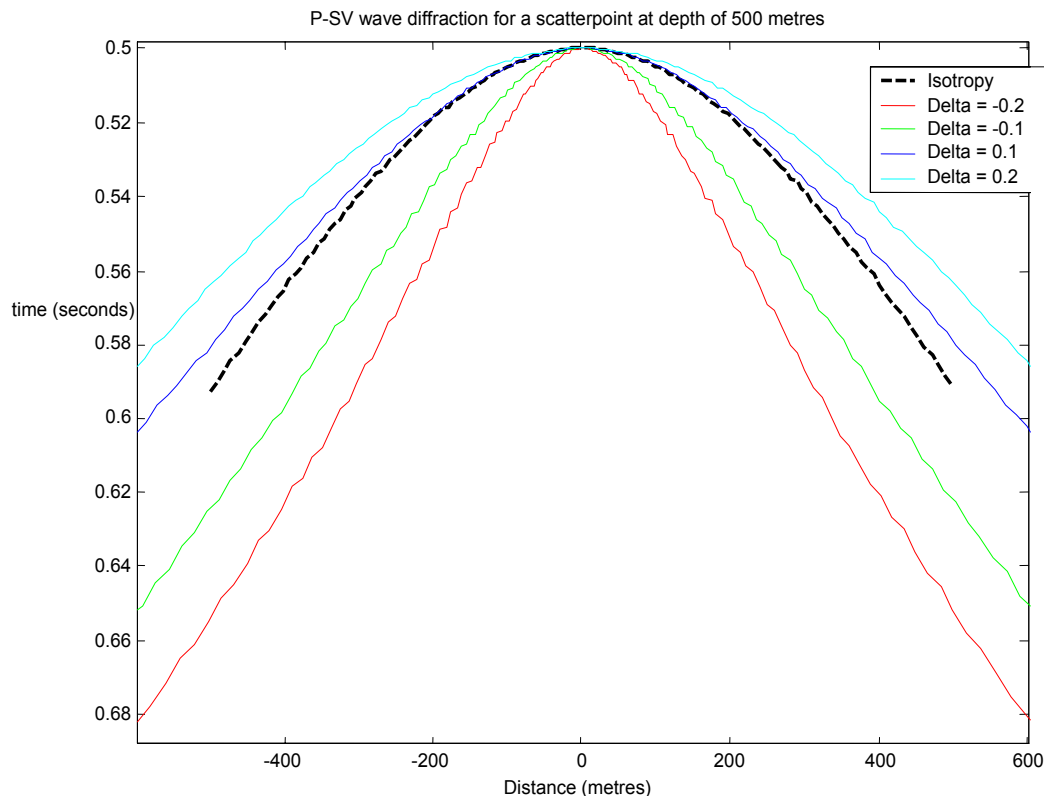

FIG. 17. Expected diffraction shapes for converted waves from a scatterpoint at located at 500m

Inspection of Figure 17 shows, as expected, that the diffraction from a scatterpoint at 500 metres is asymmetrical and rough.

NON-HYPERBOLIC MOVEOUT

It is well understood that, in the presence of anisotropy, the traveltimes of waves reflected from a horizontal interface form a non-hyperbolic curve. The short-spread moveout velocity is not equal to the vertical rms velocity as in the isotropic case. For the transverse isotropic case, the moveout velocities depend on the vertical velocities and Thomsen's parameters.
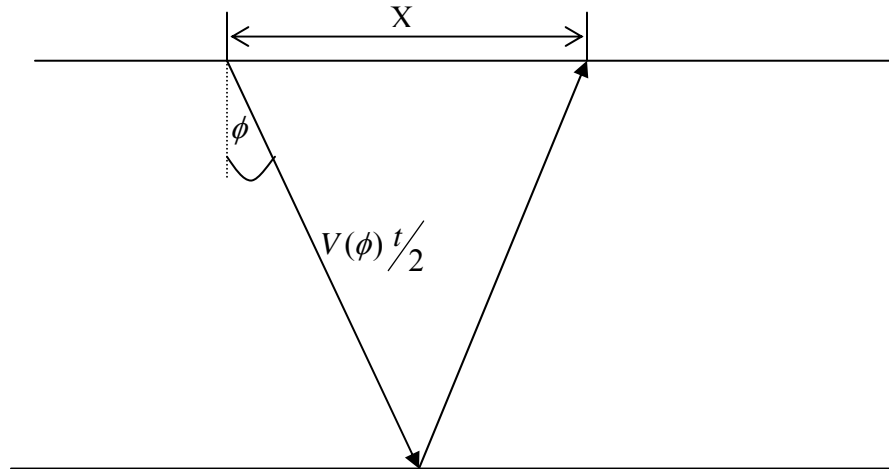
Moveout velocities

FIG. 18. Conventional reflection survey. The distance that the down-going wave travels is noted on that ray.

If a conventional reflection survey in a homogeneous anisotropic elastic medium is considered (Figure 18), the traveltime can easily be solved for from the trivial formula given below

$$\left[V(\phi)\frac{t(\phi)}{2} \right]^2 = \left[V(0)\frac{\tau}{2} \right]^2 + \left(\frac{x}{2} \right)^2, \tag{36}$$

where τ is the vertical (zero-offset) two-way traveltime, x is the source receiver offset and t is the traveltime from source to reflector to receiver. When t^2 is solved for, we obtain

$$t^2(\phi) = \left[\frac{V(0)}{V(\phi)} \right]^2 \left[\tau^2 + \frac{x^2}{V^2(0)} \right]. \tag{37}$$

Because Equation (37) is dependent on ϕ, it plots as a curved line in the $t^2 - x^2$ plane. The slope of this can be solved for

$$t^2 = \frac{V(0)^2 \tau^2 + x^2}{V(\phi)^2},$$

$$\frac{dt^2}{dx^2} = \frac{V^2(\phi) - \left(V(0)^2 \tau^2 + x^2\right)\dfrac{dV(\phi)^2}{dx^2}}{V(\phi)^4}, \qquad (38)$$

$$\frac{dt^2}{dx^2} = \frac{1}{V^2(\phi)} - \frac{t^2}{V(\phi)^2}\frac{dV(\phi)^2}{dx^2}.$$

This can be further expressed as (Thomsen, 1986)

$$\frac{dt^2}{dx^2} = \frac{1}{V^2(\phi)}\left[1 - \frac{2\cos^2\phi}{V(\phi)}\frac{dV(\phi)}{d\sin^2(\phi)}\right]. \qquad (39)$$

Normal-moveout velocity is defined using the initial slope of this line, where $V_{nmo}^2(\psi) = \lim\limits_{x\to 0}\dfrac{dx^2}{dt^2}$ and ψ is the dip angle of the reflector — in our case, 0. The ray parameter can be incorporated into this equation to ease its computational complexity, where

$$V_{NMO}^2(\psi) = \frac{2}{\tau}\lim_{x\to 0}\frac{dh}{dp}, \qquad (40)$$

where $h = x/2$ or the half-offset of the source and receiver and p is the ray parameter (Tsvankin, 1995). If we let z_0 be the depth of the zero-offset reflection point, then $h = z_0 \tan(\phi)$, Equation (40) becomes

$$V_{NMO}^2(\psi) = 2\frac{z_0}{\tau}\lim_{x\to 0}\frac{d\tan(\phi)}{dp}. \qquad (41)$$

To evaluate this equation, we use the general relations between the group and phase velocities that were developed in the group velocity section of this paper. From Equation (28), we see that the derivative $\dfrac{d\tan(\phi)}{dp}$ may be written as $\dfrac{d\tan(\phi)}{dp} = \dfrac{d\tan(\phi)}{d\theta}\dfrac{d\theta}{dp}$. Again referring to Equation (28), we see

$$\frac{d\tan\phi}{d\theta} = \frac{1 + \dfrac{1}{v}\dfrac{d^2v}{d\theta^2}}{\cos^2\theta\left(1 - \dfrac{\tan\theta}{v}\dfrac{dv}{d\theta}\right)^2}, \qquad (42)$$

and since $p = \sin(\theta)/v$,

$$\frac{d\theta}{dp} = \frac{v}{\cos\theta(1 - \frac{\tan\theta}{v}\frac{dv}{d\theta})} , \qquad (43)$$

then

$$\frac{d\tan(\phi)}{dp} = \frac{v\left(1 + \frac{1}{v}\frac{d^2v}{d\theta^2}\right)}{\cos\theta\left(1 - \frac{\tan\theta}{v}\frac{dv}{d\theta}\right)^3} . \qquad (44)$$

If we let $z_o = \frac{1}{2}V(\phi)t\cos\phi$, and use the expression for the group velocity in Equation (23b), and recall that the phase angle θ for the zero-offset ray is equal to the dip angle ψ, z_0 becomes

$$z_0 = \frac{1}{2}V(\psi)t\cos\psi\left(1 - \frac{\tan\psi}{V(\psi)}\frac{dv}{d\theta}\right). \qquad (45)$$

Substituting Equations (45) and (44) into (41), we obtain a formula for the NMO velocity

$$V_{NMO}(\psi) = \frac{V(\psi)}{\cos(\psi)}\frac{\sqrt{1 + \frac{1}{V(\psi)}\frac{d^2v}{d\theta^2}}}{\left(1 - \frac{\tan\psi}{V(\psi)}\frac{dv}{d\theta}\right)} , \qquad (46)$$

where the derivatives of the phase velocity are evaluated at the dip angle ψ of the reflector. Difficulties are expected to arise when implementing this equation for shear waves that have cusps or singularities and are therefore multi-valued. The expression in Equation (46) is fairly straightforward because it only involves the phase velocity function and the components of the group velocity. Hence for a flat reflector

$$V_{NMO}(0,P) = V_{p0}\sqrt{1 + 2\delta}$$
$$V_{NMO}(0,SV) = V_{s0}\sqrt{1 + 2\sigma} , \qquad (47)$$
$$V_{NMO}(0,SH) = V_{s0}\sqrt{1 + 2\gamma}$$

where $\sigma = \frac{V_{p0}^2}{V_{s0}^2}(\varepsilon - \delta)$ and is given by Tsvankin and Thomsen (1994). Note that σ reduces to zero for both isotropic and elliptically anisotropic media. The equations for V_{NMO} are equal to the rms velocity when the anisotropic parameters (σ, δ and γ) are all zero. As expected, the SH-wave is completely decoupled from the P and SV-waves. In a homogeneous transversely isotropic medium, as is the case that we dealt with in this paper, the wavefront of the SH-wave is always elliptical and therefore the SH-moveout is

purely hyperbolic. The reflection moveout for an SH-wave will however become non-hyperbolic for a stratified medium.

Reflection Traveltimes

A common approximation for reflection moveouts is the Taylor-series expansion of the $t^2(x^2)$ curve near $x^2 = 0$ (Taner and Koehler, 1969).

$$t_T^2 = A_0 + A_2 x^2 + A_4 x^4 + ..., \tag{48}$$

where $A_0 = \tau^2$, $A_2 = \left[\dfrac{dt^2}{dx^2}\right]_{x=0}$ and $A_4 = \left[\dfrac{1}{2}\dfrac{d}{dx^2}\left(\dfrac{dt^2}{dx^2}\right)\right]_{x=0}$. For a P wave, these parameters are solved for as

$$A_2(P) = \frac{1}{V_{P0}^2(1-2\delta)} \quad ; \tag{49a}$$

$$A_4(P) = \frac{-2(\varepsilon-\delta)}{\tau_{P0}^2 V_{P0}^4} \frac{1 + \dfrac{2(\varepsilon-\delta)}{1 - \dfrac{V_{S0}^2}{V_{p0}^2}}}{(1+2\delta)^4}$$

and for the SV case,

$$A_2(SV) = \frac{1}{V_{S0}^2(1-2\sigma)} \quad . \tag{49b}$$

$$A_4(SV) = \frac{2\sigma}{\tau_{s0}^2 V_{S0}^4} \frac{1 + \dfrac{2\delta}{1 - \dfrac{V_{S0}^2}{V_{p0}^2}}}{(1+2\sigma)^4}$$

A receiver spread is said to be short if it is not greater than the depth of the reflector. The short-spread moveout velocity is expressed through the inverse of A_2. Note that for all three wave types the short-spread moveout velocity is generally different from the true vertical velocity. The SV-wave short-spread moveout velocity is determined by the parameter σ, which may be much bigger than the anisotropy parameters because of the squared velocity ratio. Subsequently, the short-spread SV-wave moveout may be more distorted by anisotropy than the P-wave. Traditionally the Taylor-series expansion is truncated after the second term, where the effective stacking velocity is equal to the short spread limit.

INTERMEDIATE SPREAD AND THE WEAK ANISOTROPIC MOVEOUT

From Figure 18 it is seen that

$$t(\phi) = \frac{V_0 \tau}{V(\phi)\cos\phi} , \tag{50}$$

where τ is now the two-way traveltime. Assuming the anisotropy is weak, and following Thomsen (1986), we can use the weak anisotropic approximation where we equate the group velocity at ϕ to the phase velocity at θ. These approximations are seen in Equations (30) and (34) and have been developed earlier in this paper. For t^2, we now have

$$t^2(\phi) = \frac{\tau^2}{\cos^2\phi(1 + 2\delta\sin^2\phi\cos^2\phi + 2\varepsilon\sin^4\phi)} , \tag{51}$$

where the expression for the square of the velocity has been approximated through a binomial series. Expressing the group angle through x and z, and further linearizing in the anisotropy parameters, we get

$$t^2(\bar{x}^2) = \tau^2\left[1 + \bar{x}^2\left(1 - 2\frac{\delta}{1+\bar{x}^2}\right) - \bar{x}^4\frac{2\varepsilon}{1+\bar{x}^2}\right], \tag{52}$$

where the offset has been normalized such that $\bar{x} = \dfrac{x}{2z} = \dfrac{x}{Vo\tau}$.

It is clear that Equation (52) has the form a Taylor series expanded in x^2. We then arrive at the final weak anisotropic approximation for the traveltime curve.

$$t^2 = \tau^2 + A_2^w x^2 + \frac{A_4^w x^4}{1 + \left(\dfrac{x}{V_0\tau}\right)^2} , \tag{53}$$

where $A_2^w(P) = 1 - \dfrac{2\delta}{V_{p0}^2}$,and $A_4^w(P) = -\dfrac{2(\varepsilon - \delta)}{\tau^2 V_{p0}^4}$ for the P-wave. Note the similarities of A_4 to the expressions in Equation (49a), where the first part of the term constitutes the approximation. In a similar fashion, formulas for the SV wave can be developed. Equation (53), as anticipated, is only valid under the condition of weak anisotropy.

LONG-SPREAD REFECTION MOVEOUT

The three-term Taylor series gives important information about the behaviour of nonhyperbolic moveout, but it loses accuracy with increasing offset and has an increasing error for $x_{max} > 1.5z$ (Tsvankin & Thomsen, 1994). This should not be surprising since the equation reflects the shape of the traveltime curve near the zero-offset or at small incidence angles. A better analytical approximation may be formed if the traveltimes defined by the three-term Taylor series (Equation (49)) and weak anisotropy (Equation (53)) are amalgamated:

$$t^2 = \tau^2 + A_2 x^2 + \frac{A_4 x^4}{1 + A x^2}, \qquad (52)$$

where A_2 and A_4 are the same as in Equation (49), $A = \dfrac{A_4}{\dfrac{1}{V_h^2} - A_2}$, and V_h is the horizontal

incidence velocity. The parameter A has been introduced to ensure the proper behaviour at large offsets.

SYNTHETIC MOVEOUT RESULTS

The traveltimes were calculated using three different methods — ray-tracing, the Taylor-series expansion for large spreads, and using a best-fit hyperbola. The value of ε was kept constant at 0.160 and the value of δ was allowed to vary. Figures 19 and 20 show the results obtained for a horizontal reflector located at a depth of 500 metres. The solutions are calculated for incident angles that range from zero to forty-five degrees (note that the critical angle was not considered).
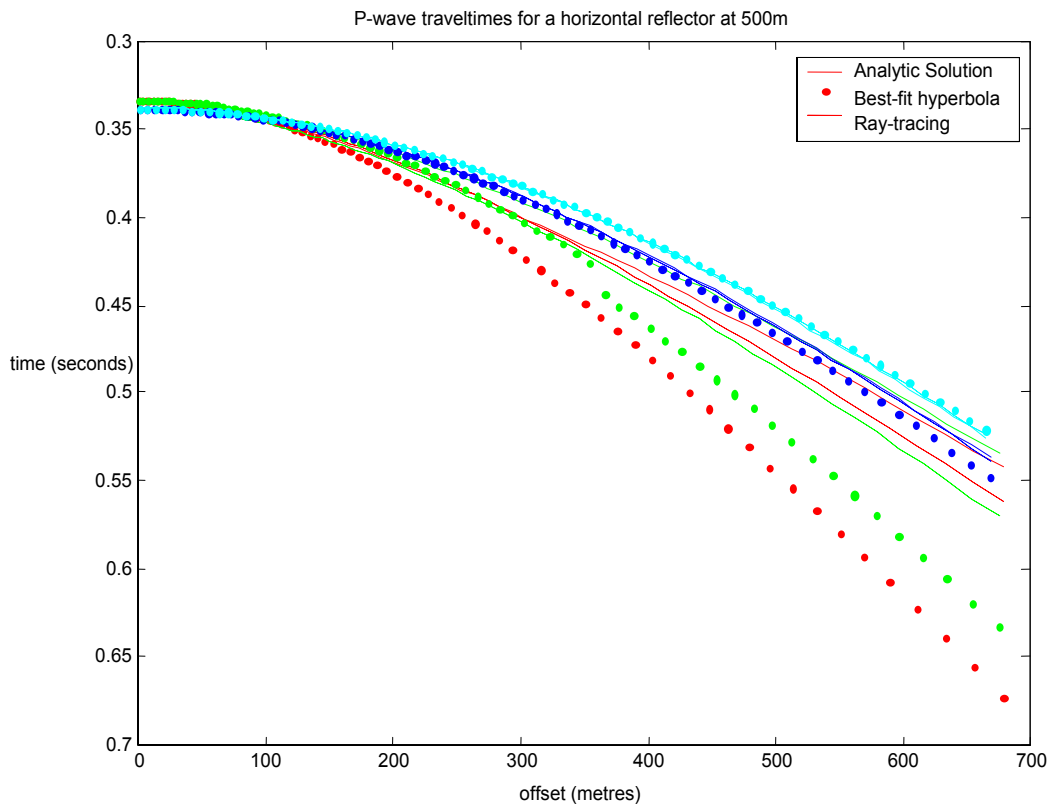

FIG. 19. P-wave two-way traveltime for a horizontal reflector located at a depth of 500 metres. The traveltime was calculated using three different methods as annotated on the graph. The red lines correspond to a δ = -0.2, the green line to δ = -0.1, the blue line to δ = 0.1, and the cyan line to δ = 0.2. ε was held constant at 0.160.

We see that the analytic solution best approximates the solution obtained by ray-tracing. For both the analytic solution and the best-fit hyperbola, the greatest deviation from the ray-tracing method is seen at the largest offsets and both approximations deviate more from the true solution when the δ is negative.
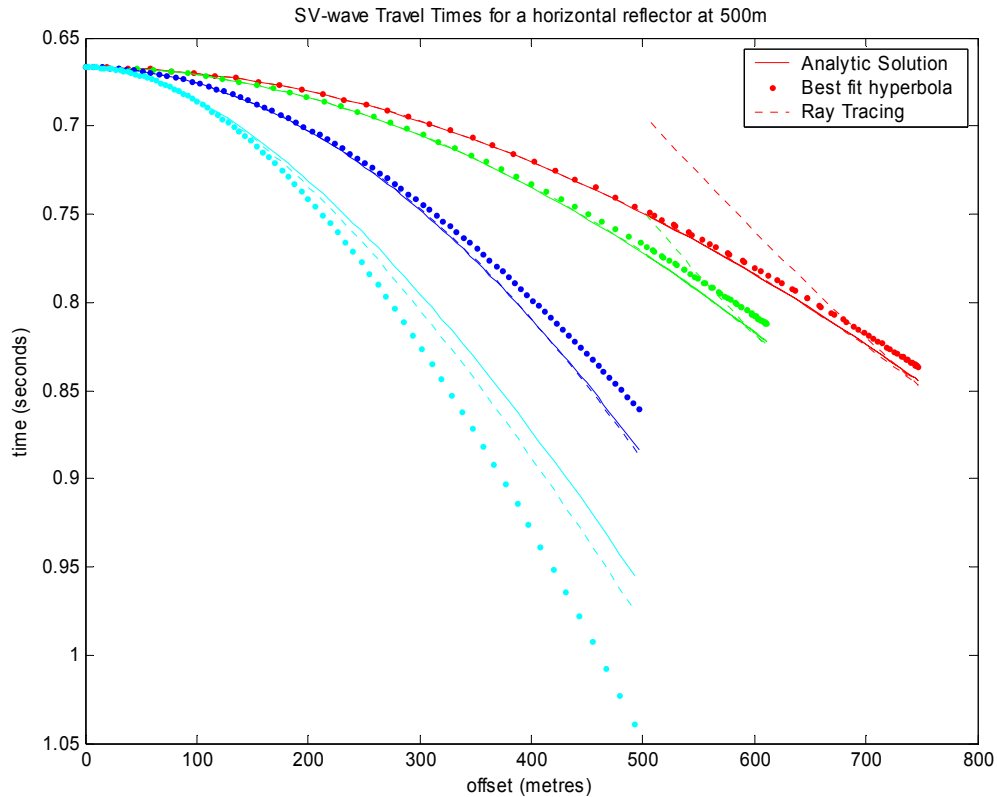

FIG. 20. SV-wave two-way traveltime for a horizontal reflector located at a depth of 500 metres. The traveltime was calculated using three different methods as annotated on the graph. The red lines correspond to δ = -0.2, the green line to δ = -0.1, the blue line δ = 0.1, and the cyan line to δ = 0.2. ε was held constant at 0.160. Neither the analytic solution or the best-fit hyperbola are able to image past the first arm of the cusp.

Similar observations are seen for the SV-wave case as for the P-wave case. An important limitation of both methods for the SV-wave is that neither the analytic solution nor the best fit hyperbola are able to simulate more than the first arm of the cusp that is evident in some SV-wave traveltime curves.

On short spreads, the moveout remains close to hyperbolic even in the presence of anisotropy. The waves diverge from being hyperbolic with increasing $|\varepsilon - \delta|$ and with decreasing δ.

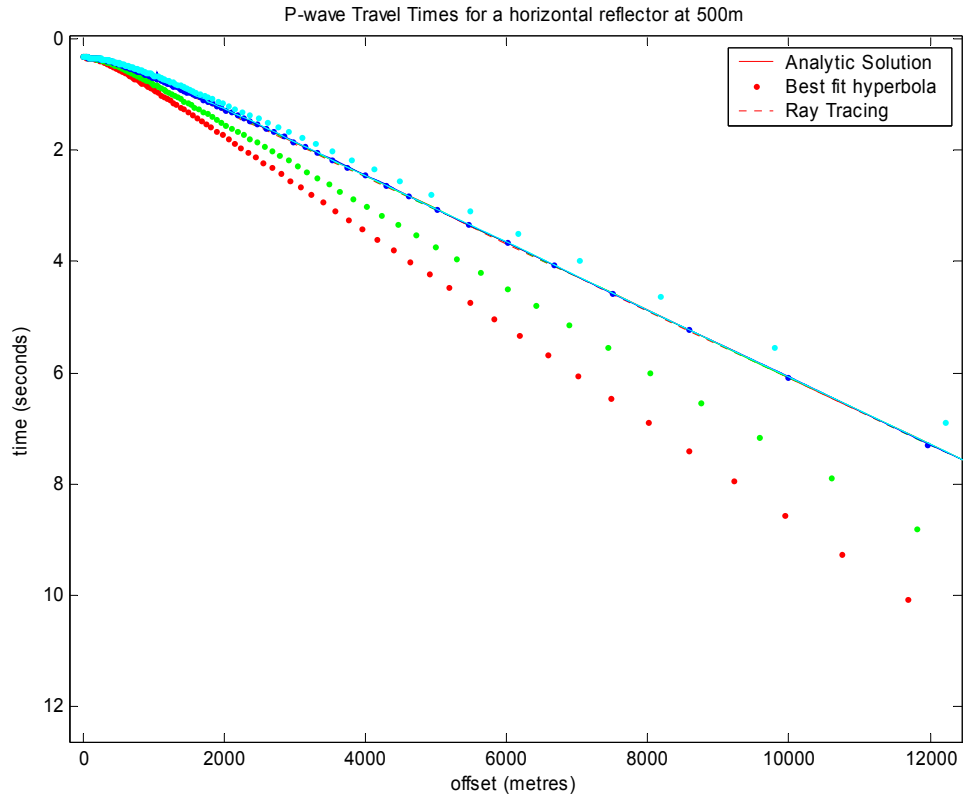Examination of Figures 21 and 22 shows how these calculations behave for long offsets.

FIG. 21. P-wave traveltimes for long offsets calculated using three different methods — ray-tracing, an analytic solution, and a best-fit hyperbola. The red lines correspond to δ = -0.2, the green line to δ = -0.1, the blue line δ = 0.1, and the cyan line to δ = 0.2. ε was held constant at 0.160.
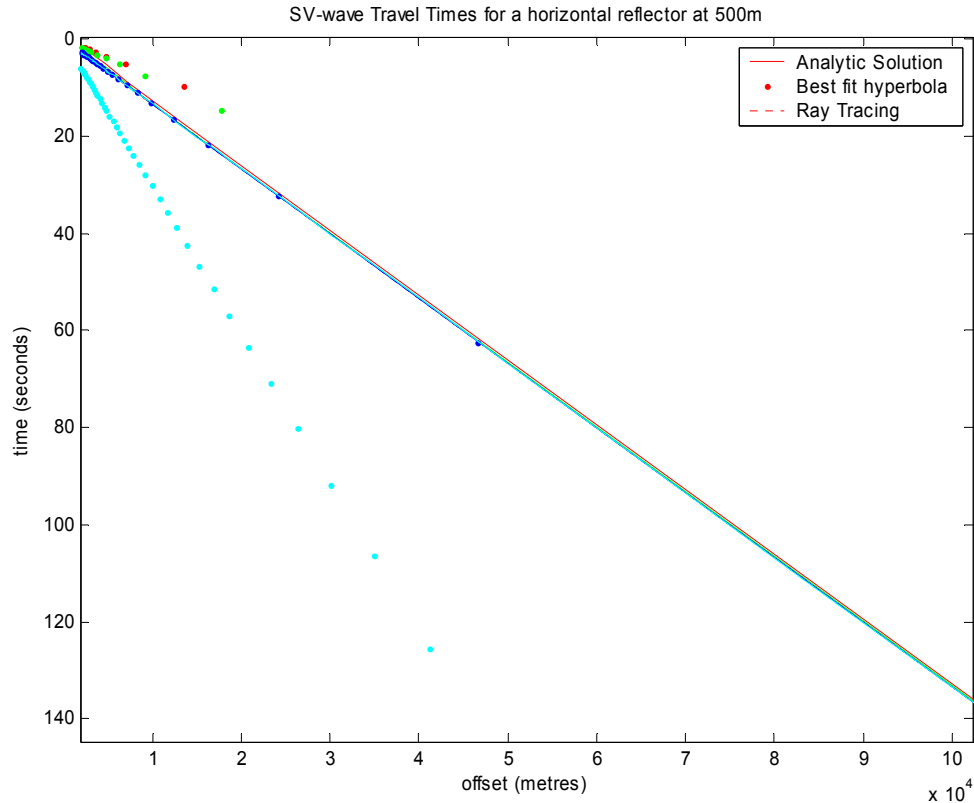
FIG. 22. SV-wave traveltimes for long offsets calculated using three different methods — ray-tracing, an analytic solution, and a best-fit hyperbola. The red lines correspond to $\delta = -0.2$, the green line to $\delta = -0.1$, the blue line $\delta = 0.1$, and the cyan line to $\delta = 0.2$. ε was held constant at 0.160.

Relative to the hyperbolic fit, the analytical solution nicely fits the ray-tracing results for both P- and SV-waves.

CONCLUSIONS

It is the anisotropy parameter δ that completely dominates near-vertical propagation for P and SV-waves and thus this parameter is the most critical when considering seismic exploration. The equations governing the weak anisotropy approximation are simpler then the more complete set of equations but are not always accurate; this is especially evident in the SV-wave. Because of the power of today's computers there is no excuse to use an approximation and all such programs should be developed with the more exact equations in mind so that one is not skimping on accuracy.

REFERENCES

Byun, B.; 1984, Seismic parameters for transversely isotropic media: Geophysics, **49**, 1908–1914.

Daley, P.F., and Hron, F., 1977, Reflection and transmission coefficients for transversely isotropic media for converted waves: Geophys. Prosp., **36**, 671–688.

Love, A.E.H., 1927, A Treatise on the Mathematical Theory of Elasticity: Dover Publications, Inc.

Shearer, P.M.; 1999, Introduction to Seismology: Cambridge University Press.

Taner, M.T., and Koehler, F., 1969, Velocity spectra-digital computer derivation and applications of velocity functions: Geophysics, **34**, 859–881.

Tessmer, G., and Behle, A.F., 1988, Common reflection point data stacking technique for converted waves: Geophys. Prosp., **36**, 671–688.

Thomsen, L.; 1986, Weak elastic anisotropy: Geophysics, **51**, 1954–1966.

Tsvankin, I., and Thomsen, L., 1994, Nonhyperbolic reflection moveout in anisotropic media: Geophysics, **59**, 1290–1304.

Tsvankin, I., 1995, Normal moveout from dipping reflectors in anisotropic media: Geophysics, **60**, 268–284.

Yilmaz, O., 1987, Seismic Data Analysis: Processing, inversion, and interpretation of seismic data: Society of Exploration Geophysicists.